Published in final edited form as:
Invest Ophthalmol Vis Sci. 2008 August ; 49(8): 3677–3686. doi:10.1167/iovs.07-1071.

Synaptic Pathology in Retinoschisis Knockout (*Rs1*$^{-/y}$) Mouse Retina and Modification by rAAV-*Rs1* Gene Delivery

Yuichiro Takada[1], **Camasamudram Vijayasarathy**[1], **Yong Zeng**[1], **Sten Kjellstrom**[1], **Ronald A. Bush**[1], and **Paul A. Sieving**[1,2]

[1] *Section for Translational Research in Retinal and Macular Degeneration, National Institute on Deafness and Other Communication Disorders (NIDCD), Bethesda, Maryland* [2] *National Eye Institute (NEI), National Institutes of Health, Bethesda, Maryland*

Abstract

Purpose—At an early age, the retinoschisin knockout (*Rs1*-KO) mouse retina has progressive photoreceptor degeneration with severe disruption of the outer plexiform layer (OPL) that decreases at older ages. The electroretinogram (ERG) undergoes parallel changes. The b-wave amplitude from bipolar cells is reduced disproportionately to the photoreceptor a-wave at young but not at older ages. The protein expression and morphology of the OPL in *Rs1*-KO mice was investigated at different ages, to explore the role of the synaptic layer in these ERG changes.

Methods—Retinas of wild-type (Wt) and *Rs1*-KO mice from postnatal day (P)7 to 12 months were evaluated by light and electron microscopy (EM) and biochemistry. PSD95 (postsynaptic density protein), mGluR6 (metabotropic glutamate receptor subtype 6), retinoschisin (Rs1), the Müller cell proteins glial fibrillary acidic protein (GFAP) and glutamine synthetase (GS), the bipolar cell marker protein kinase C alpha (PKCα), and the horizontal cell marker calbindin were localized by immunofluorescence and immuno-EM. Levels of PSD95 and mGluR6 were determined by quantitative Western blot. *Rs1*-KO mice treated by intravitreous injection of rAAV(2/2)-CMV-*Rs1* in one eye at P14 were evaluated at 8 months by full-field scotopic ERG responses and retinal immunohistochemistry.

Results—Rs1 was associated with the outer surface of synaptic membranes in wild-type (Wt) retinas. PSD95 and mGluR6 were juxtaposed in the OPL of the *Rs1*-KO retinas by P14, implying that synaptic structures are formed. Light microscopic retinal morphology was similar in Wt and *Rs1*-KO at P14, but by P21, the OPL was disrupted in *Rs1*-KO, and some PSD95 and mGluR6 was mislocalized in the outer nuclear layer (ONL). GFAP expression spanned all retinal layers. EM showed synaptic structures adjacent to photoreceptor nuclei. PSD95 and mGluR6 levels were normal at 1 month on Western blot but declined to 59% ($P < 0.001$) and 55% ($P < 0.05$) of Wt, respectively, by 4 months. Levels thereafter showed no further reduction out to 12 months. Eyes injected with AAV-*Rs1* were studied at 8 months by immunohistochemistry and had higher expression of PSD95 and mGluR6 and less GFAP expression compared with fellow untreated eyes.

Conclusions—In the *Rs1*-KO mouse, retinal layer formation and synaptic protein expression in the OPL is normal up to P14, implying normal development of synaptic connections. Aberrant localization of synaptic proteins by P21 indicates that displacement of developing and/or mature synapses contributes to the b-wave reduction at young ages, when photoreceptor numbers and

Corresponding author: Paul A. Sieving, National Eye Institute, National Institutes of Health, 31 Center Drive, Building 31, Room 6A03, MSC 2510, Bethesda, MD 20892; paulsieving@nei.nih.gov.

Disclosure: **Y. Takada**, None; **C. Vijayasarathy**, None; **Y. Zeng**, None; **S. Kjellstrom**, None; **R.A. Bush**, None; **P.A. Sieving**, None

synaptic protein levels are normal. The subsequent decline in PSD95 and mGluR6 between 1 and 12 months in *Rs1*-KO retina mirrors the course of b-wave change and provides evidence of causal relationship between the ERG and OPL changes. These findings and the improved structural integrity of the OPL and b-wave amplitude after *Rs1* gene transfer therapy provide a cellular and molecular basis for interpreting the changes in retinal signaling in this model. (*Invest Ophthalmol Vis Sci.* 2008; 49:3677-3686) DOI:10.1167/iovs.07-1071

X-linked juvenile retinoschisis (XLRS) is an early-onset and slowly progressive retinal and macular degeneration in young males that is caused by mutations in the *RS1* gene on the X chromosome.[1] Retinoschisin (RS1), the 24-kDa product of the *RS1* gene, is expressed in the retina and pineal gland and contains a discoidin domain.[2,3] Discoidin domains are implicated in cell adhesion and signaling.[4] Based on this, RS1 is predicted to serve as an adhesive protein in maintaining structural and functional integrity of the retina.[5] Loss of function *RS1* mutations cause splitting or schisis within the retinal layers, thinning of the ganglion and inner nuclear layers (INL),[6–8] and a very slow degeneration and loss of the photoreceptors.[9,10] Human XLRS disease frequently results in a reduced electroretinogram (ERG) b-wave relative to the a-wave, which implicates deficient responses of retinal bipolar cells postsynaptic to the photoreceptors.[7,11] Eliminating expression of the homologous *Rs1* gene ($Rs1^{-/y}$) in the *Rs1*-KO mouse model yields many characteristics of the human XLRS disease.[6,8,9]

Full molecular details of RS1 function remain elusive. Two recent studies suggested that Rs1 acts locally in the mouse retina to maintain photoreceptor and bipolar cell stability and architecture.[12,13] This would obviate the need for Rs1 to be secreted for export to the inner retina, as previously proposed.[14] We reported that Rs1 is bound by anionic phospholipids on the photoreceptor inner segment membrane surface[12] and suggested that the loss of Rs1 on inner segments contributes to the displacement and disorganization of photoreceptors in the *Rs1*-KO retina.[12] Molday et al.[13] subsequently reported that Rs1 is associated with Na^+/K^+-ATPase and SARM1 complex on photoreceptor and bipolar cell membranes. However, the role of Rs1 in maintaining retinal synaptic connectivity is not yet clear.

Our previous study of changes in retinal morphology and the ERG with age in *Rs1*-KO mice showed a steady decrease in photoreceptor cell number with age, but unlike other photoreceptor degeneration models,[15–17] there was a disproportionate b-wave reduction compared with the photoreceptor a-wave, and the b-/a-wave ratio (b-/a-wave ratio) decreased between 1 and 4 months.[9] At later ages, the b-wave decline slowed, even though the number of photoreceptor cells declined substantially, actually causing the b-/a-wave ratio to increase. This phenomenon suggests that factors affecting synaptic signaling or bipolar cell function during this period, in addition to photoreceptor cell loss, affect the ERG. We investigated the role of outer plexiform layer (OPL) synapses in b-wave response changes in the *Rs1*-KO mouse by studying the changes in synaptic protein expression in *Rs1*-KO retina during postnatal development and into adulthood and also after treatment by AAV-mediated *Rs1* gene delivery.

MATERIALS AND METHODS

Animals

Age-matched C57BL/6 Wt ($Rs1^{+/y}$) and *Rs1*-KO ($Rs1^{-/y}$) mice ranging in age from 7 days to 12 months were used in the study. *Rs1*-KO mice were generated in our laboratory from C57BL/6 blastocytes, as described previously.[6,9] The animal experiments were conducted in accordance with the National Institutes of Health (NIH) Animal Care and Use Committee protocols and the ARVO Statement for the Use of Animals in Ophthalmic and Vision Research.

Antibodies

The Rs1 antibody used is an affinity-purified polyclonal antibody raised in guinea pigs against a synthetic peptide corresponding to the N-terminal amino acid residues 24–37 (stedegedpwyqka) conserved between murine and human species.[2] The other primary antibodies used in this study are mouse anti-PSD95 (BD Biosciences, Franklin Lakes, NJ); rabbit anti-mGluR6 (Novus Biologicals, Littleton, CO); rabbit anti-synaptophysin (Abcam, Cambridge, MA); mouse anti-PKCα (Santa Cruz Biotechnology, Inc., Santa Cruz, CA); mouse anti-GFAP (Sigma-Aldrich, St. Louis, MO); mouse anti-Calbindin (Sigma-Aldrich); and rabbit anti-NMDA receptor subunit 1 (NR1; Millipore, Billerica, MA).

Tissue Preparation for Histology

Eyes from age-matched Wt and *Rs1*-KO mice were collected at postnatal day (P)7, P14, and P21 and at 1, 2, 4, and 12 months. The mice were deeply anesthetized with intraperitoneal ketamine (80 mg/kg)/xylazine (4 mg/kg) and perfused transcardially with 4% paraformaldehyde (PFA) in 0.1 M phosphate buffer (PB, pH 7.4). The fixed eye tissues were removed immediately and immersed in the same fixative for 2 to 4 hours and rinsed in PBS at 4°C overnight. For frozen sections, whole eyes were cryoprotected in 30% sucrose/PBS and embedded in OCT compound (Tissue Tek; EM Sciences, Fort Washington, PA). For sections evaluated by confocal microscopy, tissue was embedded in 5% agarose/PBS.

Histology

Frozen sections obtained from Wt and *Rs1*-KO retinas at P7, P14, and P21 were stained with hematoxylineosin (HE) for light microscopy and photomicrography. (Eclipse E800; Nikon Instruments Inc., Melville, NY). For electron microscopy (EM) analysis, microtome sections from 4-month-old *Rs1*-KO mice were dehydrated in ethanol in series (30%, 50%, 70%, and 96%), block-stained in 1% uranyl acetate in absolute ethanol for 1 hour, rinsed in 2× absolute ethanol, and then embedded via propylene oxide in epoxy resin (Embed 812; EM Science). Ultrathin sections were prepared (Ultracut UC6 Ultramicrotome; Leica Microsystems, Bannockburn, IL) and stained in two steps with uranyl acetate and lead citrate. The sections were examined with a transmission electron microscope (model 1010; JEOL USA, Inc., Peabody, MA) operated at 80 KeV. Electron micrographs of six to eight subdivisions per section were taken at ×2,500 and ×10,000 magnifications.

Immunohistochemistry

For single labeling, retinal sections from P7, P14, and P21 and 4-month-and 8-month-old Wt and *Rs1*-KO mice were incubated overnight at 4°C with one of the primary antibodies: Rs1 (1:500), PSD95 (1:1000), mGluR6 (1:500), synaptophysin (1:1000), PKCα (1:500), GFAP (1:500), or calbindin (1:500). After washing in PBS, retinal sections were incubated with appropriate secondary antibodies labeled with Alexa 488 or Alexa 568 (Invitrogen Corp., Carlsbad, CA). The incubation media also contained 4′,6-diamidino-2-phenylindole (DAPI) to counter-stain nuclear DNA. For double labeling, retinal sections were incubated with the following antibody cocktails: PSD95/calbindin, PSD95/PKCα, and mGluR6/PKCα. Stained retinal sections were analyzed under a confocal laser scanning fluorescence microscope (TCS SP2; Leica Microsystems, Bannockburn, IL). For pre-embedding immuno-EM, microtome sections from 2-month-old Wt and 4-month-old Wt and *Rs1*-KO were cut at 50-μm thickness and incubated for 48 hours with anti-Rs1 or anti-mGluR6 antibody. Primary antibody binding was detected with 1.4-nm gold-conjugated anti-guinea pig or -rabbit secondary IgGs (Nanoprobe, Stony Brook, NY). For examination by low magnification transmission EM, the immunogold particles were enlarged by a hydroquinone-based silver enhancement kit (Nanoprobe). The samples were then treated with 1% osmium tetroxide, stained en bloc with 1% uranyl acetate, dehydrated in ethanol and propylene oxide, and then embedded in resin

(Embed 812; EM Science, Hatfield, PA). Ultrathin sections were observed by transmission EM (JEOL USA) at magnifications of ×2,500 and ×10,000 and operating at an accelerating voltage of 80 KeV.

Synaptosome Preparation

Synaptosomes were isolated from retinas of 8- to 10-week-old C57BL/6 mice.[18] Retinas were removed and homogenized in three volumes of ice-cold HME buffer (20 mM HEPES [pH 7.4], 1 mM $MgCl_2$, 0.1 mM EGTA, 1 mM DTT, and protease inhibitor cocktail) in an all-glass homogenizer (Dounce; Bellco Glass Corp., Vineland, NJ), and the homogenates were centrifuged at 900*g* for 10 minutes at 4°C to pellet the nuclei and unbroken cells. The postnuclear supernatant was centrifuged at 12,000*g* for 20 minutes, to pellet the crude synaptosomal fraction. The pellet was resuspended in buffer A (320 mM sucrose, 5 mM Na-HEPES/HCl; pH 7.4) and layered on a discontinuous gradient of 1.2, 1.0, and 0.85 M sucrose prepared in buffer A. After centrifugation for 2 hours at 110,000*g* in a rotor (SW60 Ti; Beckman Coulter, Inc., Fullerton, CA), the synaptosomes were collected at the 1.0 to 1.2 M interphase, washed, and resuspended in buffer A.

Membrane Extraction

Preparation of whole-cell lysates from Wt mice retinas and the alkaline and high-salt extraction of membrane fractions were performed as described previously.[12] The retinal membrane fractions (100 μg protein) were adjusted to 50 mM Na_2CO_3, 0.3 and 1 M KCl by the addition of respective stock solutions of 1 M Na_2CO_3 and 3 M KCl, and incubated on ice for 15 minutes with occasional vortexing. The insoluble fraction was pelleted by layering the mixture over 0.6 M sucrose and centrifuging it at 100,000*g* (TLA 100.2 rotor; Beckman) for 30 minutes. The pellets were solubilized in Laemmli sample buffer, whereas the supernatants were first precipitated in trichloroacetic acid and then solubilized in Laemmli sample buffer. The pellets and the supernatant fractions were adjusted to equal volumes and analyzed for Rs1 by Western blot analysis using standard protocols.

Western Blot Analysis

Whole-cell lysates were prepared from Wt and *Rs1*-KO mice retina by the freeze-thaw method in a lysis buffer (10 mM Tris-HCl [pH 7.4], 150 mM NaCl, 1% Triton X-100, 1 mM EDTA, 1 mM EGTA, and 0.5% Igepal CA 630 plus protease inhibitor cocktail). The lysates were resolved on sodium dodecyl sulfate–polyacrylamide gel electrophoresis (SDS-PAGE) and electrophoretically transferred to polyvinylidene fluoride (PVDF) membrane (Bio-Rad Laboratories, Hercules, CA). After the reaction was blocked with 5% skim milk, the membranes were incubated overnight with one of the following antibodies: rabbit anti-Rs1 (1:1000), mouse-anti-PSD95 (1:1000), mouse anti-synaptophysin (1: 1000), rabbit anti-NMDA receptor subunit 1 (NR1, 1:500), or rabbit anti-mGluR6 (1:500). The membranes were then incubated with horse-radish peroxidase–conjugated anti-mouse or anti-rabbit secondary antibodies (GE Healthcare, Piscataway, NJ). The targeted proteins were detected and quantified by using enhanced chemiluminescence reagents (Pierce Biotechnology, Rockford, IL) and quantified (Image Station 200R; Eastman Kodak Co., Rochester, NY). To confirm the loading equivalency of the protein in each sample, the blots were reprobed with anti-β-actin (1:2000). The relative protein levels were calculated from the band intensity of each protein normalized to β-actin band intensity and expressed as ratios. Data were analyzed for statistical significance by two-way ANOVA (Prism; Graph Pad, San Diego, CA). $P \leq 0.05$ was considered significant.

Adenovirus-Associated Vector Preparation and Gene Delivery by Intravitreous Injection

The Cis pAAV(2/2)-CMV-*Rs1* vector, in which the *Rs1* cDNA was driven by the CMV promoter, was made by inserting the 705-bp *Eco*RI fragment of the pCR-*Rs1* plasmid into the *Eco*RI restriction site of the pZac2.1 vector (Vector Core, Division of Medical Genetics; University of Pennsylvania Health System, Philadelphia, PA). We previously reported using this vector for *Rs1* gene delivery into *Rs1*-KO mouse retina.[6,9] The *Rs1*-KO mice were anesthetized, and intravitreous injections were performed with a 33-gauge needle, as previously described.[6,19] Each of the three *Rs1*-KO mice of postnatal age 14 days were given 1.5 μL of AAV-*Rs1* (rAAV-Rs1) at a titer of 2.3×10^{10} GC/μL into the right eye, and the left eye served as the control. After a period of 8 months, the retinal function of these mice was examined by electroretinogram (ERG) recordings before the eyes were enucleated and examined by light microscopy.

Electroretinogram (ERG)

Full-field scotopic ERGs were recorded from rAAV-*Rs1*–injected male *Rs1*-KO and age-matched C57bl/6 (Wt), as previously described (n = 3 each).[9] Mice were dark-adapted for 12 hours before anesthesia with intraperitoneal administration of ketamine (80 mg/kg) and xylazine (4 mg/kg). The pupils were dilated with topical 0.5% tropicamide and 0.5% phenylephrine HCl. Mice were placed on a heating pad to maintain body temperature near 38° C while ERGs were recorded. A stimulus intensity range of −6.9 to +2.4 log cd-s/m^2 was obtained with neutral-density filters (Oriel, Stratford, CT). Responses were amplified 5000 times and filtered at 0.1 Hz to 1 kHz with a 60-Hz line-frequency filter (CP511 AC amplifier; Grass-Telefactor Division, Astro-Med., West Warwick, RI).

RESULTS

Localization of Retinoschisin in Retinal Synapse

Biochemical analysis of synaptosomes isolated from Wt retina (Fig. 1A) showed that Rs1 was highly enriched in the synaptic membrane fraction and pelleted along with the synaptic markers PSD95 and synaptophysin. Rs1 was not detected in the cytosol. Denaturing with high pH using 100 mM Na_2CO_3 released Rs1 from the membrane, indicating that it was a loosely adherent peripheral protein, whereas proteins with high affinity for membranes (PSD95) or with transmembrane domains (NMDA receptor subunit 1; NR1) remained bound to the membrane in the pellet (Fig. 1B). Thus, Rs1 is affiliated with the outer surface of the synaptic membrane.

Immunogold EM of the OPL for Rs1 showed particles on the plasma membrane surface of rod spherules and cone pedicles, but not in the cytosol (Fig. 2). Particles were also on the invaginating bipolar cell processes and distributed around the bipolar dendrites. Rs1 immunogold particles were localized on the plasma membrane of IPL dyad synaptic complexes (Fig. 2C) but were not seen on the synaptic ribbon.

Histologic Evaluation of the *Rs1*-KO Retina during the Postnatal Development

Developmental changes in retinal structure were examined in Wt and *Rs1*-KO mice at ages P7, P14, and P21 (Fig. 3). P7 *Rs1*-KO retinas (Fig. 3J) showed no major changes in morphology compared with age-matched Wt (Fig. 3A). However, at P14, the INL had multiple small schisis cavities (Fig. 3K), and by P21, the size of these cavities had increased and extended into the OPL (Fig. 3L).

GFAP is synthesized by two classes of retinal glial cells: astrocytes in the ganglion cell layer constitutively express GFAP, whereas Müller cells express GFAP only after injury.[20] In Wt retina, GFAP labeling was restricted to the ganglion cell and nerve fiber layers from P7 through P21 (Figs. 3D–F), consistent with earlier observations that GFAP is not found in retinal cells

other than astrocytes during normal development.[20] Müller cell processes labeled with antibodies to glutamine synthetase (GS) were present from P7 to P21 in Wt and *Rs1*-KO but were irregular at P14 and P21 in *Rs1*-KO retinas (Figs. 3Q, 3R). GFAP labeling of Müller cells in *Rs1*-KO retina at P7 was similar to that in Wt, with expression limited to the retinal surface (Fig. 3M). However, by P14, GFAP was seen throughout the inner half of the *Rs1*-KO retina (Fig. 3N), indicating Müller-cell-reactive gliosis in response to injury, and by P21, GFAP expression extended across the entire retina (Fig. 3O).

Changes of Pre- and Postsynaptic Markers in *Rs1*-KO (*Rs*$^{-/y}$) Retina

The altered ERG b-wave pattern in *Rs1*-KO suggests a synaptic transmission failure. We explored this possibility with pre- and postsynaptic markers in the OPL. In Wt retina at P14 and P21, processes of horizontal cells labeled with calbindin Ab and rod bipolar cells labeled with PKC*α* Ab were associated with PSD95-immunolabeled rod axon terminals in the OPL (Figs. 4A, 4B, 4D, 4E). mGluR6 in the postsynaptic membrane was proximal to presynaptic PSD95 labeling (Figs. 4C, 4F). At P14, the *Rs1*-KO retina showed a similar colocalization of presynaptic photoreceptor terminals with rod bipolar and horizontal cell processes and juxtaposition of mGluR6 and PSD95, indicating normal contacts between pre- and postsynaptic cell types (Figs. 4G–I). However, by P21 the OPL of *Rs1*-KO was irregular, and horizontal cell and rod bipolar cell processes and mGluR6 labeling extended into the ONL along with PSD95-labeled photoreceptor terminals (Figs. 4J–L). These results indicate that disrupted OPL and displaced synaptic structures occur after normal layer formation and synaptogenesis in the OPL.

In an earlier study, we had observed increasing disruption and cavity formation in the OPL and INL in *Rs1*-KO between 1 and 4 months of age, and the disruption was associated with a decrease in b-/a-wave ratio.[9] Photoreceptor loss also began to occur during this period. However, although the number of photoreceptors continued to decline up to 12 months, the number of cavities peaked and the b-/a-wave ratio reached a minimum at 4 months, after which cavities decreased and the b-/a-wave ratio increased. We looked at 4-month-old retinas to learn whether these changes are reflected at the synapse. Photoreceptor synaptic proteins PSD95 and synaptophysin were abundant in the OPL of Wt retina (Fig. 5), but were considerably reduced in *Rs1*-KO, as indicated by reduced im-munostaining intensity. Some PSD95 was mislocalized outside the OPL, as seen at P21 in *Rs1*-KO, and EM confirmed the presence of synaptic ribbons in the ONL adjacent to photoreceptor nuclei (Fig. 5E). mGluR6 immunostaining was also reduced in 4-month-old *Rs1*-KO (Fig. 6). Double labeling Wt retina with PKC*α* showed juxtaposition of rod bipolar termini with copious mGluR6 postsynaptic punctate labeling (Fig. 6). In the *Rs1*-KO retina, mGluR6 punctate labeling was reduced disproportionate to PKC-*α* staining of bipolar cell processes. Some synaptic terminals were certainly formed in the *Rs1*-KO retina, evidenced by green dots of mGluR6 labeling at the tips of PKC-*α*-labeled bipolar cell processes. Many other bipolar termini, however, appeared to lack mGluR6 labeling at the tips, and some processes extended into the ONL (Fig. 6F). At the ultrastructural level mGluR6 immunoreactivity was mislocalized within bipolar cell dendrites rather than on the synaptic plasma membrane (Fig. 6I). Others have observed mGluR6 aberrantly in rod bipolar cells and axons in *crx*$^{-/-}$ retina.[21] These results indicate that two alterations in the OPL, the reduction of synaptic proteins and mislocalization of synaptic structures could contribute to the reduced ERG b-wave amplitude in *Rs1*-KO retina.

Western blot analysis of whole-cell lysates indicated significant reduction of PSD95 and mGluR6 at 4 and 12 months and in PSD95 at 2 months in *Rs1*-KO compared with Wt (Fig. 7A, 7B; $P < 0.001$, two-way ANOVA, Bonferroni posttest, $n = 3$ per age). PSD95 and mGluR6 declined significantly between 1 and 4 months to 59% and 55% of Wt, respectively ($P < 0.05$, one-way ANOVA, Bonferroni posttest), but showed no further significant decline between 4

and 12 months (Fig. 7B). Likewise, ERG b-wave data replotted from our earlier study[9] in Figure 7 showed a significant decrease in amplitude proportional to WT between 1 and 4 months ($P < 0.05$), but no decrease between 4 and 12 months. In contrast, the ONL width (representative of photoreceptor number) showed a consistent decline with age, which was significant only between 1 and 12 months ($P < 0.05$).

We used the b-/a-wave ratio to explore the response of postsynaptic neurons (b-wave) in the ERG adjusted for the input these neurons receive from the photoreceptors. A small b-/a-wave ratio indicates reduced postsynaptic activity relative to photoreceptor output. In *Rs1*-KO mice the b-/a-wave ratio decreased between 1 and 4 months but then increased to above the Wt ratio by 12 months of age.[9] When we plotted the quantity of synaptic proteins (adjusted for photoreceptor cell number) in *Rs1*-KO, we observed a pattern of change with age similar to the b-/a-wave ratio (Fig. 7C), with a low point occurring at 4 months and a significant increase between 4 and 12 months ($P < 0.005$, one-way ANOVA, Bonferroni posttest). Figure 7C suggests that synaptic protein levels declined faster than photoreceptor numbers between 1 and 4 months, though the decline in the ratio did not reach the level of statistical significance. Thus, the disproportionate reduction of the ERG b-wave amplitude (postphotoreceptor activity) compared to a-wave (photoreceptor activity) in *Rs1*-KO may result from more rapid changes in synaptic structure than loss of photoreceptor responses. The significant increase of protein levels between 4 and 12 months compared with the number of photoreceptors ($P < 0.01$) serves as a marker for the relative preservation of synaptic structure during this period. It mirrors the increase in postsynaptic compared with photoreceptor responses between 4 and 12 months, as measured by the ERG ($P < 0.01$), again suggesting a causal relationship.

Partial Restoration of Synaptic Integrity in the *Rs1*-KO Retina

Previous studies showed that reprovisioning the Rs1 protein via gene delivery using an AAV-CMV-*Rs1* (rAAV-*Rs1*) construct delivered to the developing retina at 14 days of age[9] and also to a 3-month-old adult *Rs1*-KO mouse resulted in a larger b-wave amplitude.[6] We considered whether this therapeutic effect might reflect changes in synaptic structure and PSD95 and mGluR6 expression. We administered an AAV vector that contained the murine *Rs1* cDNA driven by a CMV promoter to the right eyes of three *Rs1*-KO mice by intravitreous injection at 14 days of age and performed ERG analysis and histology 8 months later. Figure 8 shows a representative outcome. The untreated *Rs1*-KO eye showed an abnormal dark-adapted ERG waveform with the b-wave reduced more than the a-wave. By contrast, the rAAV-injected eye showed a larger b-wave amplitude resulting in an essentially normal b- and a-wave configuration (Fig. 8C). The photoreceptors were not fully rescued, but the treated eye had more cells remaining than the untreated eye (Fig. 8P–R).

After rAAV-*Rs1* delivery Rs1 protein was found in the OPL (Fig. 8F), though at reduced levels compared with Wt (Fig. 8D), and mGluR6 and PSD95 expression was increased, as judged by qualitative immunolabeling intensity (Figs. 8I, 8L, 8O), compared to untreated retinas (Figs. 8H, 8K, 8N), indicating a partial preservation of rod-bipolar synapses in the treated retina in parallel with the improved ERG (Fig. 8C). Fluorescent GFAP immunolabeling was diminished in the treated retina (Figs. 8P–R). As XLRS disease results in glial hypertrophy and proliferation,[22,23] the effect of *Rs1* gene delivery indicates a retinal reparative process driven by the presence of the Rs1 protein. Reducing GFAP expression itself has been shown to protect retinas from degeneration.[24] In the least, providing Rs1 protein to the *Rs1*-KO retina by the AAV-CMV construct was not deleterious.

DISCUSSION

Rs1 expression occurs early in postnatal development of the mouse retina and by P7 is apparent in the newly formed OPL.[2] However, the present results demonstrate that disruption of the

OPL does not occur in mice without functional Rs1 until after synaptic proteins are correctly localized. However, Rs1 appears to be needed for preservation of synaptic structures in the OPL at later ages. The ectopic localization of pre- and postsynaptic processes and synaptic terminal proteins outside the OPL as early as P21, before photoreceptor loss, implicates a loss of Rs1 function at the OPL in these disruptive changes. Alternatively, these changes could result from disruption of the photoreceptors and ONL, such as displacement of nuclei into the outer–inner segment region as early as 1 month,[9] which physically distort OPL structures.

The b-wave amplitude of *Rs1*-KO mice is reduced 50% compared to a 32% reduction in the a-wave at 1 month,[9] which suggests that OPL disruptions, including mislocalization of synaptic structures occurring before measurable loss of synaptic protein, contribute to the b-wave decline at this age. Synaptic proteins decreased faster than the number of cells in the ONL between 1 and 4 months (Fig. 7C). While the decline in the ratio of synaptic proteins to ONL was not statistically significant, it exactly paralleled the decline in the b-/a-wave ratio, representing postsynaptic relative to photoreceptor function. Even in an XLRS model without a decrease in the a-wave until 4 months—the splice site mutant *Rs1h*^{tmgc1} mouse—the b-wave amplitude is greatly decreased, and synaptic disorganization is present in the OPL as early as P17.[25] These observations suggest that the early effects on synaptic structure contribute to the functional deficit reflected in the b-wave reduction and helps explain why the XLRS model differs from other models of photoreceptor degeneration, such as the rhodopsin P23H[15,17] and RCS rat[16] which show greater loss of the a- than b-wave. Synaptic alterations are seen in those models, but only after extensive photoreceptor loss occurs.[26,27]

The major pathologic feature of the retina of the *Rs1*-KO mice is the loss of integrity of OPL, INL, and photoreceptor cells. Both bipolar and photoreceptor cells express Rs1. Despite the deficiency of Rs1 in *Rs1*-KO bipolar cells, the IPL appears morphologically intact, suggesting that bipolar axons are targeted correctly to IPL. However, their physiological competence is not fully known. These observations support the idea that the defect at the OPL is due to photoreceptor disease, which can be seen by 1 month of age.[9] In the present study, no OPL structural abnormality was observed in *Rs1*-KO at P14, the age of peak synaptogenesis in mouse.[28] Photoreceptors, particularly the outer segments, are normally maturing between P14 and P21,[29] and in our model and the splice site mutant, *Rs1h*^{tmgc1} mouse, OPL structures began to be affected during this same period, providing a further link between photoreceptor and synaptic disease in Rs1-deficient mice.

The close association of Rs1 with the photoreceptor inner segment membrane and disruption of the plasma membrane and intracellular structures in *Rs1*-KO mouse[12] indicates normal photoreceptor function requires Rs1. Photoreceptor disease as the origin of synaptic dysfunction has been suggested for the *Rs1h*^{tmgc1} mouse, which has a milder phenotype than our *Rs1*-KO mouse.[25] Axonal degeneration or axonal retraction stemming from a defect in photoreceptor homeostasis has been suggested as a mechanism of synaptic loss in several other murine genetic models: (1) nob2 mouse with a null mutation in a subunit of the L-type calcium channel (*Cacna 1f*),[30] (2) β2 subunit of the voltage-dependent calcium channel (VDCC),[31] and (3) mice lacking expression of bassoon.[32] All these mutant mouse models share features of XLRS disease: disrupted OPL, ectopic synapses in the ONL, neurite outgrowth from bipolar and horizontal cells, and a reduced ERG b-wave. It has been suggested that the ectopic extension of rod bipolar and horizontal cell dendrites into the ONL reflects mechanical tension generated by the retracting axon.[33] Axonal degeneration is emerging as a contributor of retinal dysfunction, even in retinal degenerations in which the primary defect is not in a synaptic protein, such as age-related macular degeneration and in the aging retina.[34,35] Of interest, ectopic synapses that are found in these presynaptic mutants are not seen in mice harboring mutations in postsynaptic proteins such as mGluR6,[36] nyctalopin,[37] or Gβo.[38] Although, a

presynaptic defect as the underlying cause of XLRS disease is consistent with a role for Rs1 in photoreceptor homeostasis, this possibility was not resolved by the present study.

Presynapatic (PSD95) and postsynaptic (mGluR6) protein as well as the b-/a-wave ratio reached a minimum at 4 months and then increased significantly ($P < 0.01$) and in parallel between 4 and 12 months. Thus, despite continuing photoreceptor loss, the level of synaptic proteins and responses from second-order neurons increased relative to photoreceptor number and function. This implies some form of OPL synaptic plasticity. Relative preservation of postsynaptic ERG responses has been observed in at least two other models of photoreceptor degeneration: the rhodopsin P23H rat[15] and the RCS rat[16] at the bipolar and amacrine cell levels, respectively. However, in *Rs1*-KO this preservation occurs only at a relatively late stage of photoreceptor degeneration and at a time when other more visible spontaneous structural improvements are occurring, including the regression of cavities and improvements in photoreceptor layer organization,[9] making this model unique.

At all stages, at least some of the synapses had appropriate pre- and postsynaptic molecular constituents PSD95 and mGluR6 that were juxtaposed, indicating apparently intact synapses. The ERG correlate is that, although the *Rs1*-KO b-wave is small, responses can still be elicited with dim stimuli, even near normal threshold, demonstrating synaptic transmission between photoreceptors and rod ON-bipolar cells.[9] Affected human XLRS males have only a modest elevation of absolute luminance threshold after dark adaptation,[11] and the elevation is less severe than would be expected in most other forms of retinal degeneration from the degree of reduction in rod-mediated b-wave amplitude. This is consistent with deficient signaling from rods to rod bipolar cells or deficient function of rod bipolar cells in XLRS.

Plasticity of the Photoreceptor Synapse after AAV-Mediated *Rs1* Gene Transfer

rAAV-mediated *Rs1* gene transfer at P14 under the CMV promoter leads to ubiquitous expression of the Rs1 protein and partially restores retinal function in the *Rs1*-KO model and increases the levels of synaptic proteins, including mGluR6. Since AAV-mediated gene expression reaches a maximum only at 4 to 6 weeks after intravitreous injection of AAV vector,[39,40] *Rs1* gene transfer at P14 would not immediately arrest early degeneration processes, as they begin in the OPL by P14 to P21 days. Nevertheless, as we observed in a previous longer term study,[9] *Rs1* gene delivery at an early age slows the degenerative process and preserves the number of photoreceptor cells into late age. Consistent with those findings, the present study demonstrates at the molecular level a better organized OPL and the presence of the synaptic proteins after AAV-*Rs1* application, and the ERG b-wave amplitude was enhanced accordingly.[6,41] Since reactive gliosis is thought to be a clinically significant limiting factor in recovery of vision after retinal injury,[42–45] suppression of GFAP levels in the treated *Rs1*-KO retina may facilitate recovery.[24]

These results indicate that *Rs1* gene therapy results in synaptic protein expression as well as molecular rearrangements that appear to facilitate ERG-b wave improvement. Such plasticity of adult neuronal contacts is well known[46] and has also been demonstrated for the photoreceptor synapse with diurnal light stimulation.[47] The significant functional and structural improvement observed at the molecular level in the retina of the treated mice indicates that the *Rs1*-KO retinal synapses remain in a dynamic state and can rearrange in response to the retinoschisin molecule. It remains to be determined, however, to what extent this translates into restoring vision, per se.

Note Added in Proof

Recently Wang et al. (*Eur J Neurosci.* 2008;27:2177–2187) demonstrated withdrawal of photoreceptor terminals and sprouting of bipolar and horizontal cell dendrites into the ONL,

where they appeared to form ectopic synapses with rods, in the retinas of mice treated with vigabatrin, a GABA-transaminase inhibitor. The similarity to the *Rs1*-KO retina, including regions of ONL where rod nuclei were displaced outward toward the RPE, is evidence that the mislocalization of OPL synaptic proteins in our study is associated with the withdrawal of photoreceptor terminals and sprouting of post synaptic dendrites into the ONL.

Acknowledgements

The authors thank Maria Santos-Muffley for technical assistance and Juanita Marner for assistance in manuscript preparation.

Supported by the NIH Intramural Research Program through NIDCD and NEI.

References

1. Sauer CG, Gehrig A, Warneke-Wittstock R, et al. Positional cloning of the gene associated with X-linked juvenile retinoschisis. Nat Genet 1997;17:164–170. [PubMed: 9326935]
2. Takada Y, Fariss RN, Tanikawa A, et al. A retinal neuronal developmental wave of retinoschisin expression begins in ganglion cells during layer formation. Invest Ophthalmol Vis Sci 2004;45:3302–3312. [PubMed: 15326155]
3. Takada Y, Fariss RN, Müller M, Bush RA, Rushing EJ, Sieving PA. Retinoschisin expression and localization in rodent and human pineal and consequences of mouse RS1 gene knockout. Mol Vis 2006;12:1108–1116. [PubMed: 17093404]
4. Vogel W. Discoidin domain receptors: structural relations and functional implications. FASEB J 1999;13(suppl):S77–S82. [PubMed: 10352148]
5. Wu WW, Wong JP, Kast J, Molday RS. RS1, a discoidin domain-containing retinal cell adhesion protein associated with X-linked retinoschisis, exists as a novel disulfide-linked octamer. J Biol Chem 2005;280:10721–10730. [PubMed: 15644328]
6. Zeng Y, Takada Y, Kjellstrom S, et al. RS-1 Gene delivery to an adult Rs1h knockout mouse model restores ERG b-wave with reversal of the electronegative waveform of X-linked retinoschisis. Invest Ophthalmol Vis Sci 2004;45:3279–3285. [PubMed: 15326152]
7. Tantri A, Vrabec TR, Cu-Unjieng A, Frost A, Annesley WH Jr, Donoso LA. X-linked retinoschisis: a clinical and molecular genetic review. Surv Ophthalmol 2004;49:214–230. [PubMed: 14998693]
8. Weber BH, Schrewe H, Molday LL, et al. Inactivation of the murine X-linked juvenile retinoschisis gene, Rs1h, suggests a role of retinoschisin in retinal cell layer organization and synaptic structure. Proc Natl Acad Sci USA 2002;99:6222–6227. [PubMed: 11983912]
9. Kjellstrom S, Bush RA, Zeng Y, Takada Y, Sieving PA. Retinoschisin gene therapy and natural history in the Rs1h-KO mouse: long-term rescue from retinal degeneration. Invest Ophthalmol Vis Sci 2007;48:3837–3845. [PubMed: 17652759]
10. Bradshaw K, George N, Moore A, Trump D. Mutations of the XLRS1 gene cause abnormalities of photoreceptor as well as inner retinal responses of the ERG. Doc Ophthalmol 1999;98:153–173. [PubMed: 10947001]
11. Khan NW, Jamison JA, Kemp JA, Sieving PA. Analysis of photoreceptor function and inner retinal activity in juvenile X-linked retinoschisis. Vision Res 2001;41:3931–3942. [PubMed: 11738458]
12. Vijayasarathy C, Takada Y, Zeng Y, Bush RA, Sieving PA. Retinoschisin is a peripheral membrane protein with affinity for anionic phospholipids and affected by divalent cations. Invest Ophthalmol Vis Sci 2007;48:991–1000. [PubMed: 17325137]
13. Molday LL, Wu WW, Molday RS. Retinoschisin (RS1), the protein encoded by the X-linked retinoschisis gene, is anchored to the surface of retinal photoreceptor and bipolar cells through its interactions with a Na/K ATPase-SARM1 complex. J Biol Chem 2007;282:32792–32801. [PubMed: 17804407]
14. Reid SN, Farber DB. Glial transcytosis of a photoreceptor-secreted signaling protein, retinoschisin. Glia 2005;49:397–406. [PubMed: 15538749]

15. Aleman TS, LaVail MM, Montemayor R, et al. Augmented rod bipolar cell function in partial receptor loss: an ERG study in P23H rhodopsin transgenic and aging normal rats. Vision Res 2001;41:2779–2797. [PubMed: 11587727]
16. Bush RA, Hawks KW, Sieving PA. Preservation of inner retinal responses in the aged Royal College of Surgeons rat. Evidence against glutamate excitotoxicity in photoreceptor degeneration. Invest Ophthalmol Vis Sci 1995;36:2054–2062. [PubMed: 7657544]
17. Machida S, Kondo M, Jamison JA, et al. P23H rhodopsin transgenic rat: correlation of retinal function with histopathology. Invest Ophthalmol Vis Sci 2000;41:3200–3209. [PubMed: 10967084]
18. Luiro K, Kopra O, Lehtovirta M, Jalanko A. CLN3 protein is targeted to neuronal synapses but excluded from synaptic vesicles: new clues to Batten disease. Hum Mol Genet 2001;10:2123–2131. [PubMed: 11590129]
19. Bennett J, Duan D, Engelhardt JF, Maguire AM. Real-time, noninvasive in vivo assessment of adeno-associated virus-mediated retinal transduction. Invest Ophthalmol Vis Sci 1997;38:2857–2863. [PubMed: 9418740]
20. Sarthy PV, Fu M, Huang J. Developmental expression of the glial fibrillary acidic protein (GFAP) gene in the mouse retina. Cell Mol Neurobiol 1991;11:623–637. [PubMed: 1723659]
21. Pignatelli V, Cepko CL, Strettoi E. Inner retinal abnormalities in a mouse model of Leber's congenital amaurosis. J Comp Neurol 2004;469:351–359. [PubMed: 14730587]
22. Kirsch LS, Brownstein S, de Wolff-Rouendaal D. A histopathological, ultrastructural and immunohistochemical study of congenital hereditary retinoschisis. Can J Ophthalmol 1996;31:301–310. [PubMed: 8913633]
23. Mooy CM, Van Den Born LI, Baarsma S, et al. Hereditary X-linked juvenile retinoschisis: a review of the role of Müller cells. Arch Ophthalmol 2002;120:979–984. [PubMed: 12096974]
24. Nakazawa T, Takeda M, Lewis GP, et al. Attenuated glial reactions and photoreceptor degeneration after retinal detachment in mice deficient in glial fibrillary acidic protein and vimentin. Invest Ophthalmol Vis Sci 2007;48:2760–2768. [PubMed: 17525210]
25. Johnson BA, Ikeda S, Pinto LH, Ikeda A. Reduced synaptic vesicle density and aberrant synaptic localization caused by a splice site mutation in the Rs1h gene. Vis Neurosci 2006;23:887–898. [PubMed: 17266781]
26. Cuenca N, Pinilla I, Sauve Y, Lu B, Wang S, Lund RD. Regressive and reactive changes in the connectivity patterns of rod and cone pathways of P23H transgenic rat retina. Neuroscience 2004;127:301–317. [PubMed: 15262321]
27. Cuenca N, Pinilla I, Sauve Y, Lund R. Early changes in synaptic connectivity following progressive photoreceptor degeneration in RCS rats. Eur J Neurosci 2005;22:1057–1072. [PubMed: 16176347]
28. Blanks JC, Adinolfi AM, Lolley RN. Synaptogenesis in the photoreceptor terminal of the mouse retina. J Comp Neurol 1974;156:81–93. [PubMed: 4836656]
29. Weidman TA, Kuwabara T. Postnatal development of the rat retina: an electron microscopic study. Arch Ophthalmol 1968;79:470–484. [PubMed: 5640327]
30. Chang B, Heckenlively JR, Bayley PR, et al. The nob2 mouse, a null mutation in Cacna1f: anatomical and functional abnormalities in the outer retina and their consequences on ganglion cell visual responses. Vis Neurosci 2006;23:11–24. [PubMed: 16597347]
31. Ball SL, Powers PA, Shin HS, Morgans CW, Peachey NS, Gregg RG. Role of the beta (2) subunit of voltage-dependent calcium channels in the retinal outer plexiform layer. Invest Ophthalmol Vis Sci 2002;43:1595–1603. [PubMed: 11980879]
32. Dick O, tom Dieck S, Altrock WD, et al. The presynaptic active zone protein bassoon is essential for photoreceptor ribbon synapse formation in the retina. Neuron 2003;37:775–786. [PubMed: 12628168]
33. Fisher SK, Lewis GP, Linberg KA, Verardo MR. Cellular remodeling in mammalian retina: results from studies of experimental retinal detachment. Prog Retin Eye Res 2005;24:395–431. [PubMed: 15708835]
34. Caicedo A, Espinosa-Heidmann DG, Hamasaki D, Pina Y, Cousins SW. Photoreceptor synapses degenerate early in experimental choroidal neovascularization. J Comp Neurol 2005;483:263–277. [PubMed: 15682400]

35. Liets LC, Eliasieh K, van der List DA, Chalupa LM. Dendrites of rod bipolar cells sprout in normal aging retina. Proc Natl Acad Sci USA 2006;103:12156–12160. [PubMed: 16880381]
36. Tagawa Y, Sawai H, Ueda Y, Tauchi M, Nakanishi S. Immunohistological studies of metabotropic glutamate receptor subtype 6-deficient mice show no abnormality of retinal cell organization and ganglion cell maturation. J Neurosci 1999;19:2568–2579. [PubMed: 10087070]
37. Ball SL, Pardue MT, McCall MA, Gregg RG, Peachey NS. Immunohistochemical analysis of the outer plexiform layer in the nob mouse shows no abnormalities. Vis Neurosci 2003;20:267–272. [PubMed: 14570248]
38. Dhingra A, Jiang M, Wang TL, et al. Light response of retinal ON bipolar cells requires a specific splice variant of Galpha (o). J Neurosci 2002;22:4878–4884. [PubMed: 12077185]
39. Ferrari FK, Samulski T, Shenk T, Samulski RJ. Second-strand synthesis is a rate-limiting step for efficient transduction by recombinant adeno-associated virus vectors. J Virol 1996;70:3227–3234. [PubMed: 8627803]
40. Bainbridge JW, Mistry A, Binley K, et al. Hypoxia-regulated trans-gene expression in experimental retinal and choroidal neovascularization. Gene Ther 2003;10:1049–1054. [PubMed: 12776163]
41. Min SH, Molday LL, Seeliger MW, et al. Prolonged recovery of retinal structure/function after gene therapy in an Rs1h-deficient mouse model of x-linked juvenile retinoschisis. Mol Ther 2005;12:644–651. [PubMed: 16027044]
42. Anderson DH, Guerin CJ, Erickson PA, Stern WH, Fisher SK. Morphological recovery in the reattached retina. Invest Ophthalmol Vis Sci 1986;27:168–183. [PubMed: 3943943]
43. Erickson PA, Fisher SK, Anderson DH, Stern WH, Borgula GA. Retinal detachment in the cat: the outer nuclear and outer plexiform layers. Invest Ophthalmol Vis Sci 1983;24:927–942. [PubMed: 6862796]
44. Fisher SK, Lewis GP. Müller cell and neuronal remodeling in retinal detachment and reattachment and their potential consequences for visual recovery: a review and reconsideration of recent data. Vision Res 2003;43:887–897. [PubMed: 12668058]
45. Francke M, Faude F, Pannicke T, et al. Glial cell-mediated spread of retinal degeneration during detachment: a hypothesis based upon studies in rabbits. Vision Res 2005;45:2256–2267. [PubMed: 15924940]
46. Bliss TV, Collingridge GL. A synaptic model of memory: long-term potentiation in the hippocampus. Nature 1993;361:31–39. [PubMed: 8421494]
47. Case CP, Plummer CJ. Changing the light intensity of the visual environment results in large differences in numbers of synapses and in photoreceptor size in the retina of the young adult rat. Neuroscience 1993;55:653–666. [PubMed: 8413928]

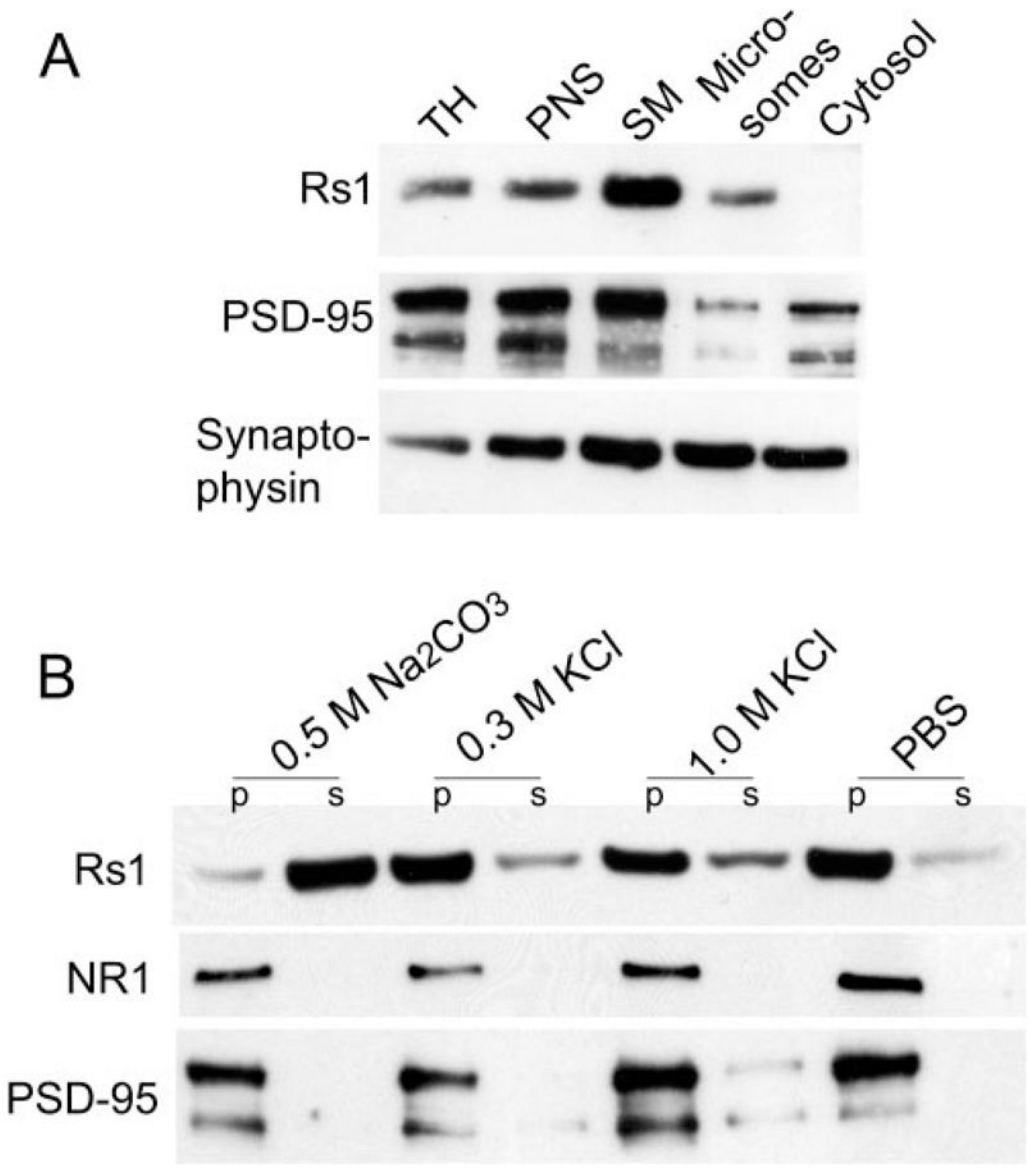

Figure 1.

Biochemical localization of Rs1 to peripheral synaptic membranes. (**A**) SDS-PAGE of subcellular fractions from mouse retina followed by immunoblot analysis. The apparent molecular weight of the proteins: Rs1, monomer 26 kDa; PSD95, ~90 kDa; and synaptophysin, 38 kDa. TH, total homogenate; PNS, postnuclear supernatant; SM, synaptic membrane. (**B**) Alkaline and high-salt extraction of the synaptic membrane fraction. Synaptic membrane (30 μg protein) fractions were incubated in the presence of Na_2CO_3 or KCl or buffer alone (PBS). After high-speed centrifugation, the membrane-associated (pellets) and solubilized (supernatants) forms of Rs1 were analyzed by immunoblot analysis. The results are representative of three independent experiments pooling two eyes from one animal for each experiment.

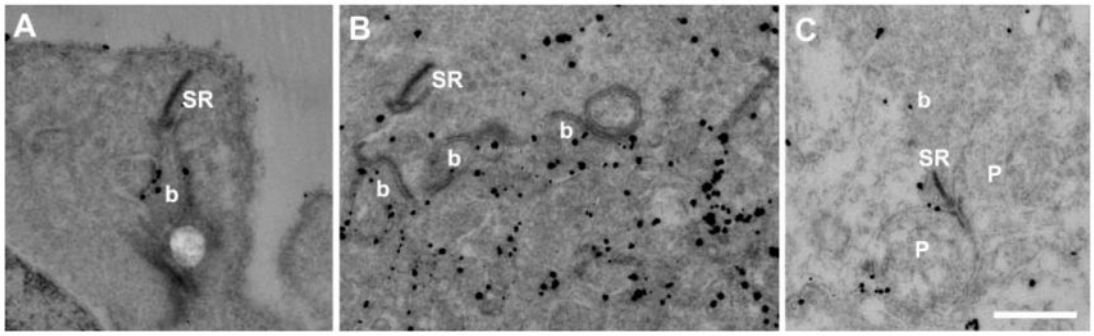

Figure 2.
Ultrastructural localization of Rs1 in the OPL and IPL. Electron micrographs of 2-month-old Wt retina immunostained with Rs1 antibody. Immunogold Rs1 particles were found in the OPL in rod spherules (**A**), cone pedicles (**B**), and bipolar cells. In the IPL, immunogold Rs1 particles were seen at the triad of bipolar and amacrine/ganglion cell processes (**C**). b, bipolar cell process; p, amacrine/ganglion process; SR, synaptic ribbon. Scale bar, 500 nm.

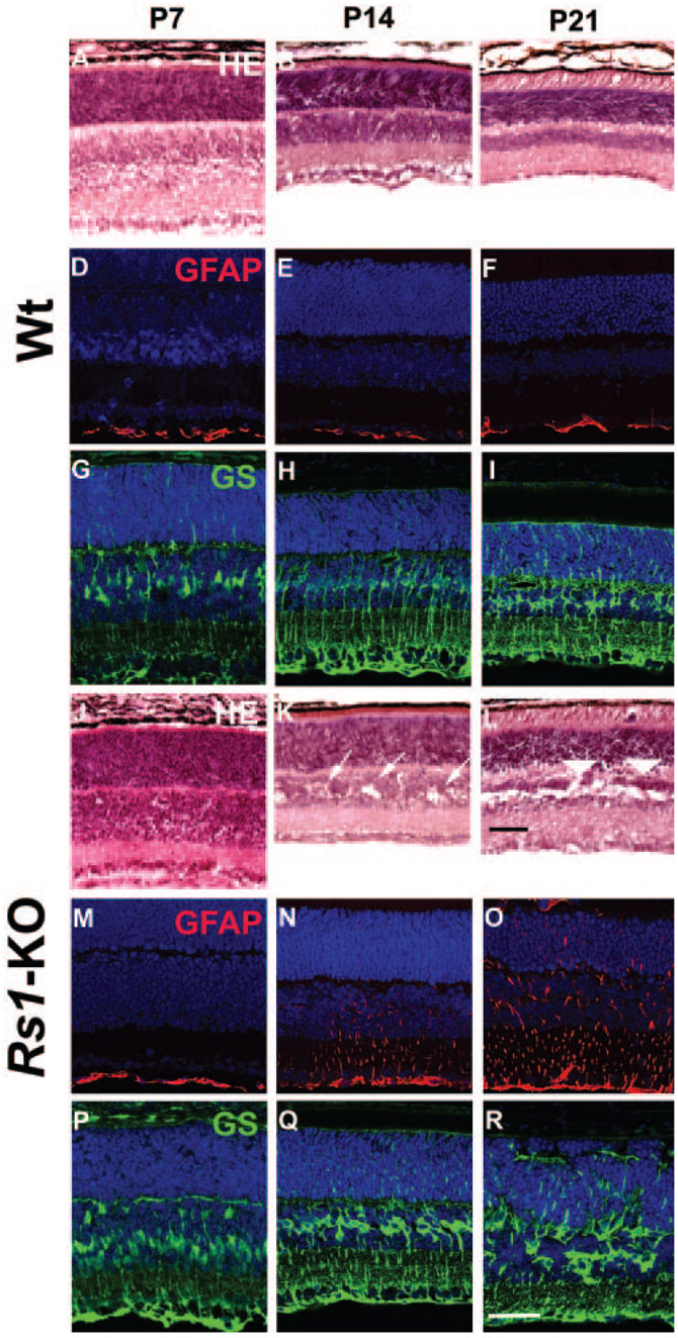

Figure 3.

Retinal morphology and glial cell immunohistochemistry of Wt and *Rs1*-KO during postnatal development. Hematoxylin and eosin–stained histology of Wt (**A**–**C**) and *Rs1*-KO (**J**–**L**) retinas at P7, P14, and P21. At P7 (**J**) no abnormal features were observed in the *Rs1*-KO retina. By P14, several schisis cavities (*arrows*) were observed in the INL of *Rs1*-KO retinas (**K**). There were no major histologic abnormalities in the OPL. In the P21 *Rs1*-KO retina, the cavities were much more extensive in the INL and were also found in the OPL (*arrowheads*) (**L**). The vacuoles in the INL of Wt retinas at P7 are processing artifacts (**A**). Müller cells and GFAP immunohistochemical staining: Müller cells, stained with GS antibody were identified at developmental stages P7, P14, and P21 (Wt, **G**–**I**; *Rs1*-KO, **P**–**R**). In Wt retina, only the nerve

fiber and ganglion cell layer showed GFAP labeling (**D**–**F**). In *Rs1*-KO retina, GFAP expression at P7 was also restricted to the nerve fiber and ganglion cell layer, but between P14 (**N**) and P21 (**O**) GFAP labeling gradually extended across all layers, which is suggestive of Müller cell hypertrophy and reactive gliosis. Scale bar, 50 μm.

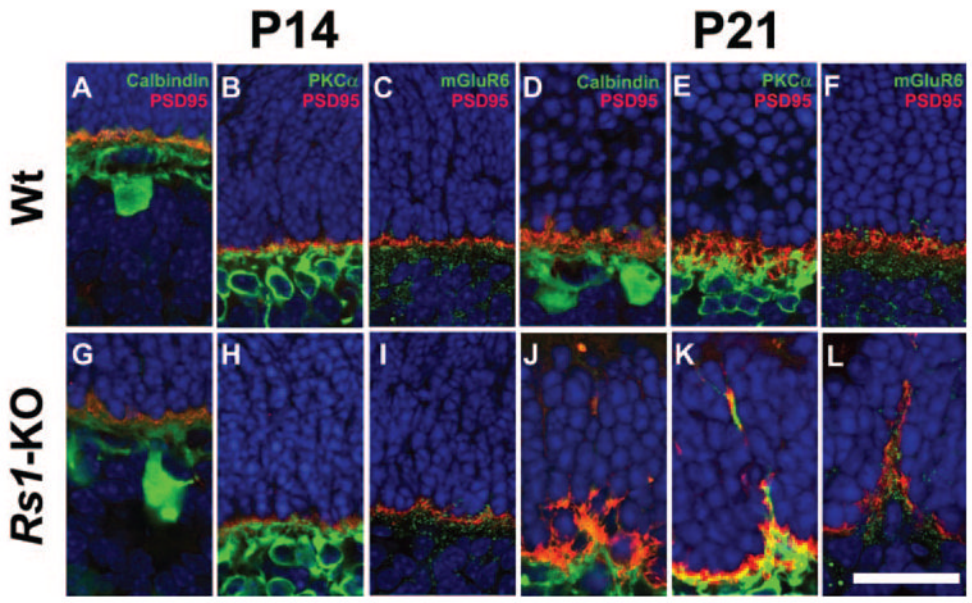

Figure 4.

Presynaptic and postsynaptic terminal labeling in Wt and *Rs1*-KO retinas during postnatal development. PSD95 (*red*) labels the photoreceptor synaptic terminal; calbindin (*green*) labels horizontal cell; PKC*α* (*green*) labels rod bipolar cell processes; mGluR6 (*green*) labels bipolar cell terminals. In Wt retina at P14 and P21, terminals of horizontal (**A**, **D**) and rod bipolar cell processes (**B**, **E**) colocalized with PSD95 immunoreactivity in the OPL. Punctate labeling of mGluR6 (*green*) and presynaptic PSD95 (*red*) were juxtaposed to each other at P14 (**C**) and P21 (**F**) in Wt retinas. *Rs1*-KO retinas at P14 showed similar staining for synaptic markers PSD95/calbindin (**G**), PSD95/PKC*α* (**H**), and mGluR6 (**I**). However, at P21 the regular arrangement of PSD95 in the OPL was disrupted in *Rs1*-KO retinas and horizontal (**J**) and rod bipolar cell (**K**) processes extended into the ONL. Aberrant extension of mGluR6 into the ONL was seen at P21 in conjunction with mislocalized presynaptic photoreceptor axons (**L**). mGluR6 and PSD95 were juxtaposed to each other at these punctate ectopic locations in the ONL. Scale bar, 25 μm

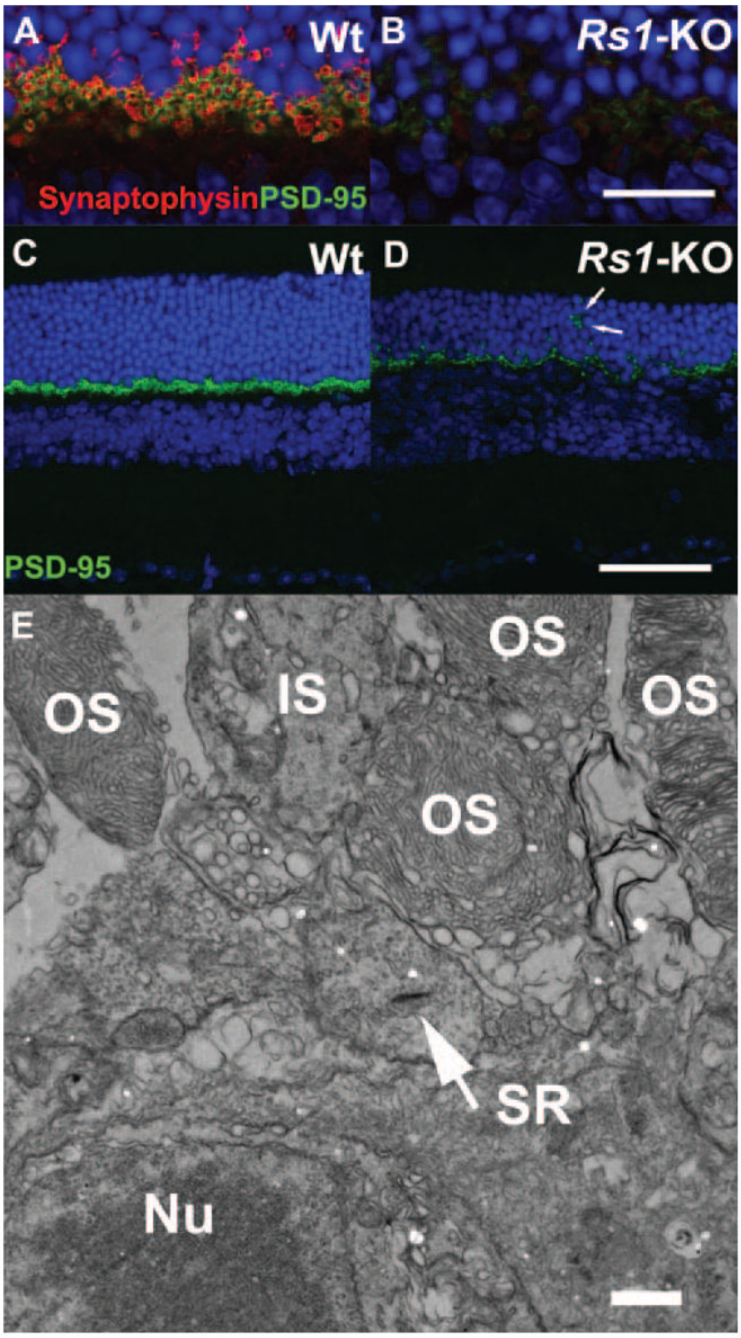

Figure 5.

Double labeling of photoreceptor synaptic terminals in 4-month-old Wt and *Rs1*-KO retinas. Wt and *Rs1*-KO mouse retinas from 4-month-old mice were stained with the presynaptic marker proteins synaptophysin (marking synaptic vesicles, *red*) and PSD95 (*green*). Labeling of both markers was greatly decreased in *Rs1*-KO retina (**B**, **D**) compared with Wt (**A**, **C**). In *Rs1*-KO, some PSD95 label was located in the ONL (**D**, *arrows*) indicating displaced terminals. At the ultrastructural level (**E**), electron microscopy confirmed displacement of photoreceptor terminals containing synaptic ribbons (SR, *arrow*) between the outer segments and nuclei of photoreceptor cells. OS, outer segment; IS, inner segment; Nu, Nuclei. Scale bar: (**A**–**D**) 75 μm; (**E**) 100 nm.

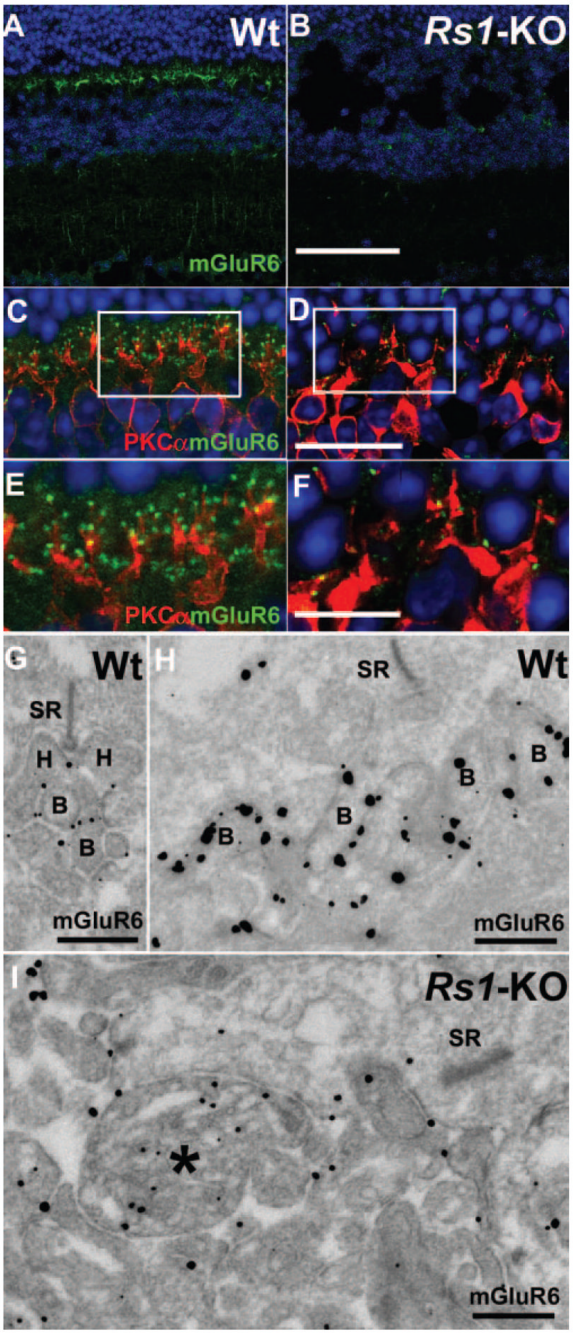

Figure 6.

Immunofluorescent staining of bipolar cell-specific markers in 4-month-old Rs1-KO retinas. Immunostaining intensity of bipolar cell mGluR6 (*green*) was greatly reduced in *Rs1*-KO mouse retina (**B**) compared with Wt at 4 months of age (**A**). Double labeling of Wt retina with PKC*α* (*red*) showed a regular network of rod bipolar cell processes colocalized with mGluR6 (**C**, **E**). In *Rs1*-KO mouse retina, PKC*α* labeling of bipolar cells dendrites are found in the ONL (**D**, **F**) along with sparse mGluR6 label (**F**). Ultrastructural localization of mGluR6 by immuno-EM showed it in the rod-bipolar (**G**) and cone-bipolar cell (**H**) plasma membrane of synaptic dendrites in 2-month-old Wt retina but mislocalized to the inside of bipolar cell dendrites (*) in *Rs1*-KO (**I**). Scale bar: (**A**, **B**) 75 μm; (**C**, **D**) 25 μm; (**E**, **F**) 12.5 μm; (**G**, **I**) 100 nm.

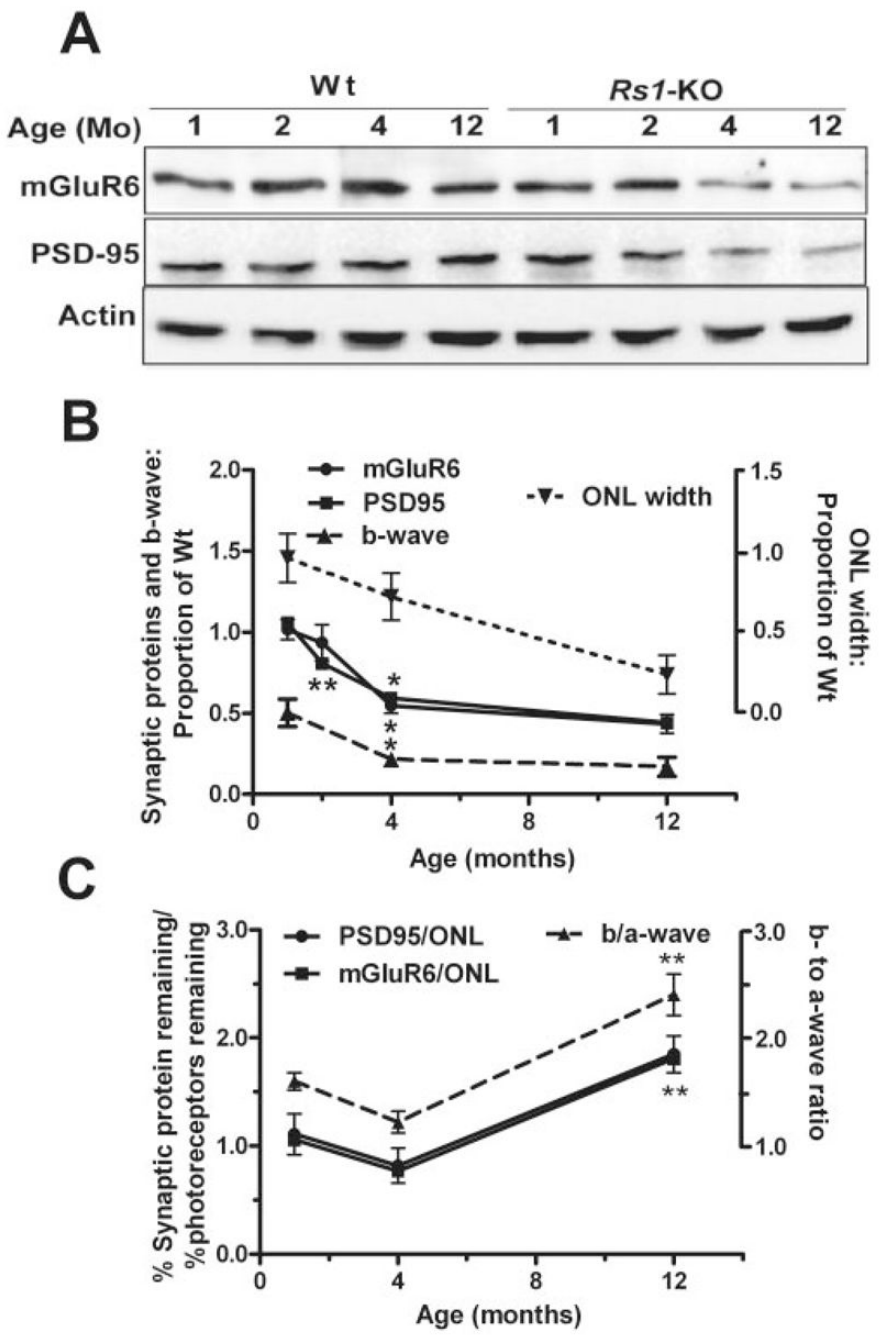

Figure 7.

Immunoblot analysis of aging changes in mGluR6 and PSD95 protein expression in Wt and *Rs1*-KO mice retinas. Representative Western blots from Wt and *Rs1*-KO mice of 1, 2, 4, and 12 months of age. The targeted proteins were detected and quantified using enhanced chemiluminescence. At 1 and 2 months of age *Rs1*-KO synaptic protein levels appeared comparable to Wt. Both PSD95 and mGluR6 protein levels declined across 2 to 12 months. (**B**) Protein levels as a proportion of Wt at each age (*solid lines*). Intensity of mGluR6 and PSD95 bands was normalized to *β*-actin band intensity, and the *Rs1*-KO value was divided by the Wt value at each age. The points were obtained from three independent experiments using a pool of two to three retinas from different mice in each experiment. The effect of age and

genotype was analyzed by two-way ANOVA and Bonferroni posttest. Differences in synaptic protein levels between Wt and *Rs1*-KO retina were statistically significant at 4 and 12 months ($P < 0.01$). Significant change from the previous age (*top asterisk* at each point, mGluR6; *bottom asterisk* at each point, PSD95: *$P < 0.05$, **$P < 0.01$, one-way ANOVA, Bonferroni posttest). For comparison to previously reported retinal morphology and ERG studies, the ONL cell count and b-wave amplitude, normalized by Wt at each age, are plotted on the same graph (*dashed lines*). (**C**) Comparison of postsynaptic response (b-wave) to synaptic protein changes with age normalized by photoreceptor responses (a-wave) or number (ONL count), respectively. The ERG values are from a previous study.[9] **Significant change from the previous age ($P < 0.01$).

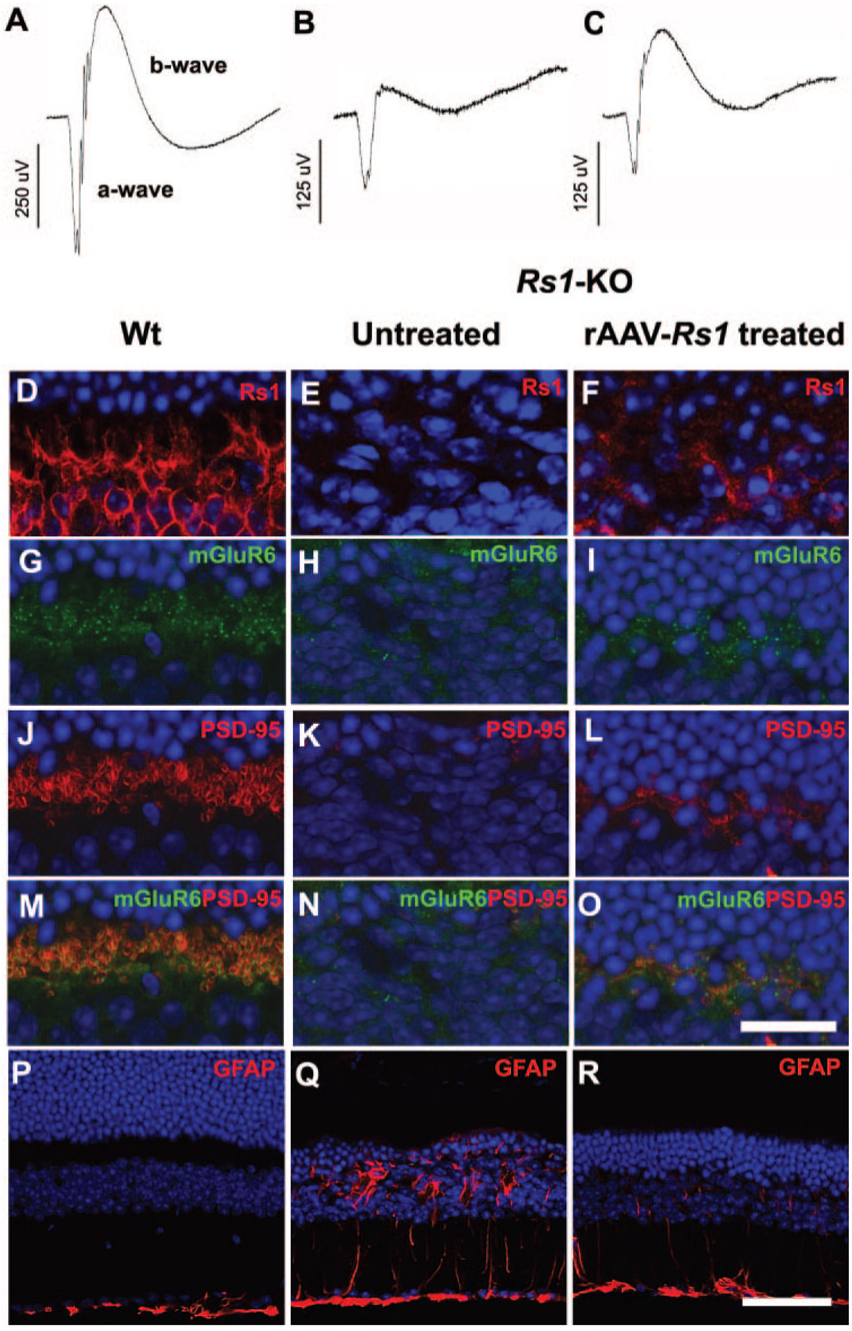

Figure 8.

ERG retinal function and synaptic structure after *Rs1* gene delivery to *Rs1*-KO retina. Representative dark-adapted ERG waveforms from an 8-month-old *Rs1*-KO mouse after gene delivery (**B**, **C**) show a larger b-wave in the treated eye, although it remains smaller than in Wt (**A**). Stimulus intensity = 0.6 log cd-s/m^2. Expression of Rs1 (*red*) was seen in the OPL of Wt retina (**D**) and rAAV-*Rs1* treated eye of the *Rs1*-KO mouse (**F**) but not in the untreated eye (**E**). Gene delivery elevated the expression levels of mGluR6 (*green*) and PSD95 (*red*) in OPL of the *Rs1*-KO retina (**I**, **L**, **O**) compared with the untreated fellow eye (**H**, **K**, **N**). Labeling of Wt retina for mGluR6, PSD95, and both mGluR6 and PSD95 is shown in (**G**), (**J**), and (**M**), respectively. Expression of GFAP (*red*) (**P**), was restricted to the inner limiting membrane in

Wt but spanned the retina of *Rs1*-KO (**Q**). rAAV-mediated *Rs1* gene delivery retina showed reduced GFAP protein expression (**R**). Scale bar: (**D**–**O**) 25 μm; (**P**–**R**) 75 μm.